THE JOURNAL OF PHYSICAL CHEMISTRY B

Article

pubs.acs.org/JPCB

Solvent-Controlled Excited State Relaxation Path of 4-Acetyl-4′-(dimethylamino)biphenyl

J. Dobkowski,* M. Kijak, I. V. Sazanovich,† and J. Waluk*

Institute of Physical Chemistry, Polish Academy of Sciences, Kasprzaka 44, 01-224 Warsaw, Poland

Supporting Information

ABSTRACT: Stationary and picosecond time-resolved fluorescence (TRF) and absorption spectra were compared in different aprotic solvents at various temperatures for 4-acetyl-4′-(dimethylamino)biphenyl (ADAB). A large value of the excited state dipole moment, 18−25 D, was estimated from the plot of solvatochromic shift. TRF spectra of ADAB recorded as a function of solvent polarity and temperature show unusual temporal evolution (shift and decay) of the fluorescence bands. In some cases, the dynamic Stokes shifts occur on a time scale much shorter than expected on the basis of literature data on solvent relaxation. In order to investigate variations in the energy of electronic transitions, oscillator strengths, and dipole moments upon changing the molecular geometry, quantum chemical modeling (DFT, TD-DFT, CIS) was performed for ADAB and its ground-state pretwisted derivative, 4-acetyl-4′-dimethylamino-2,2′-dimethylbiphenyl (ADAB-Me). Combination of spectroscopic data and computational results leads to the model of excited state relaxation which involves dynamic solvent-dependent interaction between two close-lying $^1n\pi^*$ and $^1\pi\pi^*$ excited electronic states.

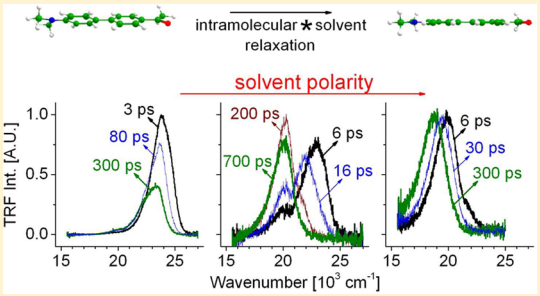

1. INTRODUCTION

Numerous molecules built of electron acceptor (A) and electron donor (D) units linked together by a single bond exhibit a peculiar behavior in their low-lying electronically excited states. The double fluorescence of 4-(dimethylamino)-benzonitrile (DMABN) was discovered more than five decades ago by Lippert and his students.[1] To explain the origin of the dual emission, these authors have postulated a solvent-induced excited state inversion of two low-lying $^1\pi\pi^*$ states: L_b and L_a. During the next two decades, the anomalous fluorescence was reported for the class of *para*-substituted molecules of the D−Ar−X type, where D is a donor, Ar is an aromatic ring, and X can be, for example, a cyano or aldehyde group. Ar−X should be treated in this case as an electron acceptor group. Alternatively, an azaaromatic ring, e.g., pyridine, was selected as the acceptor.

The Lippert model was widely accepted for over a decade until new experimental results stimulated researchers to consider alternative interpretations. During the next two decades, numerous hypotheses were proposed to explain the experimental data: (a) intermolecular interactions such as excimer or solute−solvent exciplex formation,[2−5] (b) the solvent-induced pseudo-Jahn−Teller (PJT) effect,[6] (c) the cyano group bending (RICT) mechanism,[7] (d) planarization associated with a quinoid structure (PICT/QS).[8−10] Another hypothesis, twisted intramolecular charge transfer (TICT), identifies the polar emitting state with an excited rotamer, its $-NR_2$ electron donor group being twisted by 90° with respect to the aromatic ring. A full electron transfer is assumed to occur from the amino group to the aromatic moiety.[11]

The exothermicity of the $S_1 \rightarrow$ TICT reaction occurs when the relation $E_{00} > E_{TICT} \approx E^{ox}(D) - E^{red}(A) - E_{coul}$ is fulfilled.[12] E_{00} is the electronic transition energy of the primarily excited singlet state of the molecule, $E^{ox}(D)$ and $E^{red}(A)$ are the polarographic half-wave potentials of one-electron oxidation of the donor and reduction of the acceptor, respectively, and the last term corresponds to the Coulomb stabilization energy $(-e^2/(4\pi\varepsilon_0\varepsilon r))$ of the radical pair. For 4-(dimethylamino)-acetophenone (DMAA) in acetonitrile, the relaxation to the TICT state is well established.[13−15] The replacement of the dimethylamino group (E^{ox} = 1.05 V) by *N*,*N*-dimethylaniline unit (E^{ox} = 0.65 V) should favor the $S_1 \rightarrow$ TICT reaction. 4-Acetyl-4′-(dimethylamino)biphenyl (ADAB) has *N*,*N*-dimethylaniline and acetophenone as the donor and acceptor groups, respectively (Scheme 1). Assuming that E_{coul} is similar for both molecules[12] and that the energy of the lowest singlet state can be approximated by the maximum of the lowest absorption band, the values of E_{00} can be estimated as 30800 cm^{-1} (DMAA in acetonitrile) and 28400 cm^{-1} (ADAB in acetonitrile). This indicates that the difference, $E_{00} - E_{TICT}$, is 0.1 eV (800 cm^{-1}) larger for ADAB than for DMAA, suggesting that the reaction $S_1 \rightarrow$ TICT could be a possible mechanism of the energy degradation in the case of the ADAB molecule.

On the other hand, it has been claimed that, for molecules having donor or acceptor groups with an extended π-electron

Special Issue: John R. Miller and Marshall D. Newton Festschrift

Received: October 29, 2014
Revised: December 23, 2014

DOI: 10.1021/jp510856u
J. Phys. Chem. B XXXX, XXX, XXX−XXX

Scheme 1. Compounds Investigated in This Work[a]

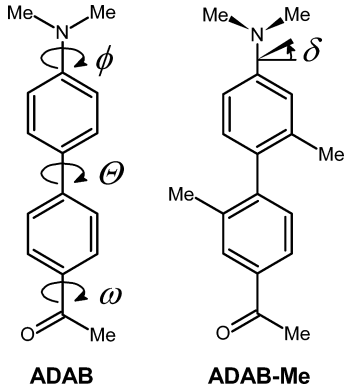

[a]The arrows indicate twist angles: ϕ, Θ, ω of the dimethylamino, *N,N*-dimethylaniline, and acetyl group, respectively; δ is the pyramidalization angle of the dimethylamino group.

system, such as pyrene[16,17] or *p*-anthryl and *p*-acridyl[18] derivatives of *N,N*-dimethylaniline, the D−A system reaches after excitation a more planar structure than that in the ground state. The photoinitiated electron transfer (ET) processes and models describing structural changes accompanying the intramolecular electron transfer (ICT) were critically analyzed and compared in the review article by Grabowski, Rotkiewicz, and Rettig.[19] Theoretical papers were published pointing to the role of conical intersections in ultrafast excited state charge separation.[20−22]

No quantum chemical calculations have been reported so far for ADAB. The calculations performed for cyano[23,24] and pyrimidine[25] analogues indicate that the mutual twist of the aromatic rings described by Θ (Scheme 1) plays the most important role. The same conclusion was reached for biphenyl derivatives with a cyano acceptor and a hydroxy or methoxy donor.[26] Because in the ground state ADAB is not planar, the value of Θ can increase or decrease after excitation. The first case suggests the relaxation to the TICT state, when *N,N*-dimethylaniline and acetophenone subgroups are mutually twisted around the central bond by 90°. In the second case, after excitation, ADAB reaches a more planar structure than that in the ground state. The goal of this work is to determine the excited state intramolecular relaxation path of ADAB and to understand the role of solvent dynamics in the energy degradation scheme.

2. EXPERIMENTAL AND COMPUTATION DETAILS

4-Acetyl-4′-(dimethylamino)biphenyl (ADAB)[27] and 4-acetyl-4′-dimethylamino-2,2′-dimethylbiphenyl (ADAB-Me)[28] were synthesized as described previously. The solvents (the list of the used solvents with their short names is given in Table 1) for absorption and emission studies (Aldrich or Merck, spectral grade) were used without further purification, except for butyronitrile (BuCN) and 2-methyltetrahydrofuran (MTHF). BuCN (Merck, for synthesis) was triply distilled over $CaCl_2$ and P_2O_5. MTHF (Merck, for synthesis) was doubly distilled over $CaCl_2$.

Stationary absorption spectra were recorded on a Shimadzu UV 3100 spectrometer. Magnetic circular dichroism (MCD) spectra were measured using an OLIS DSM 17 CD spectropolarimeter equipped with a 1.06 T permanent magnet. Stationary fluorescence spectra were measured using a Jasny[29] or FS900 Edinburgh Instruments spectrofluorimeter. The spectra were corrected for the instrumental response using fluorescence standards. Fluorescence quantum yields were determined using quinine sulfate in 0.1 N H_2SO_4 (φ_{Fl} = 0.51).[30] The fluorescence decays in the nanosecond domain were recorded with a single photon counting unit (FL 900 CDT, Edinburgh Instruments). For recording the transient absorption spectra, a home-built picosecond spectrometer was used. Briefly, pulses of 1.5 ps duration (1055 nm) and energy of 4 mJ, with a repetition rate of 33 Hz, are provided by a Light Conversion Nd:glass laser. The pulses are split into two channels. The first beam, after conversion into the third harmonic (352 nm, about 1 mJ), is used for excitation. The second beam is used for the generation of the picosecond continuum (probing beam). A home-built polychromator, equipped with a Hamamatsu back-thinned, one-stage TE-cooled CCD element (S7031-1007), is used as the detection system. The temporal resolution of the spectrometer is 2.5 ps. Time-resolved fluorescence (TRF) spectra were recorded by means of a homemade picosecond spectrofluorimeter described in detail elsewhere.[31] Briefly, the first beam, as in the setup described above, is used for excitation (352 nm). The second beam (1055 nm) passes through an optical Kerr shutter to open it. The fluorescence can be transmitted by the shutter

Table 1. Room (294 K) and Low (77 K) Temperature Fluorescence Band Maxima ($\tilde{\nu}_{max}$), Quantum Yields (φ_{Fl}), Lifetimes (τ), Radiative and Nonradiative Rates $k_f = (\varphi_{Fl}/\tau)$, $k_n = \tau^{-1} - k_f$, and Transition Dipole Moments M_f and M_a in Emission and Absorption, Respectively, Obtained for ADAB in a Number of Solvents Characterized by Polarity Index (ε) and Viscosity (η)

	solvent	ε	η^f (cP)	$\tilde{\nu}_{max}$ (cm^{-1}), 294 K	$\tilde{\nu}_{max}$ (cm^{-1}), 77 K	$\varphi_{Fl}{}^a$	τ (ns)	$k_f{}^a$ (10^9 s^{-1})	$k_n{}^a$ (10^9 s^{-1})	$M_f{}^a$ (M_a) (D)
1	*n*-hexane (HEX)	1.89	0.31	26450		0.003	0.006[b]	0.5	158	5.7 (5.1)
2	dibutyl ether (BE)	3.08	0.6	24350	24100[d]	0.11	0.290[b]	0.4	3.2	5.7
3	diisopropyl ether	3.88	0.316	23900		0.25	0.7[c]	0.36	1.1	5.7
4	diethyl ether (EE)	4.34	0.24	23000	23600	0.61	1.3[c]	0.45	0.29	6.8
5	ethyl acetate	6.02	0.429	21800		0.68				
6	terahydrofuran (THF)	7.58	0.468	21750	23400[e]	0.7	2[c]	0.35	0.15	6.3 (5.3)
7	butyronitrile (BuCN)	20.3	0.62	20250	23100	0.64	2.2[c]	0.29	0.16	6.5
8	acetonitrile (ACN)	37.5	0.35	19150		0.36	1.9[c]	0.19	0.34	5.9 (5.6)

[a]φ_{Fl} error: ±10%. For k_f, k_n, and M, the error was estimated as ±15%. $M_f = [3hk_f/64\pi^4 n^3 \tilde{\nu}_{max}{}^3]^{1/2}$, $M_a = [(3\ln 10hc)/8\pi N_A n \tilde{\nu}_{max} \int \varepsilon(\tilde{\nu})\, d\tilde{\nu}]^{1/2}$, where $\tilde{\nu}_{max}$ is the spectral position of the fluorescence or absorption band maximum, n is the refractive index, h, c, N_A are the Planck's constant, the speed of light, and the Avogadro number, respectively, and $\varepsilon(\tilde{\nu})$ denotes the molar absorption coefficient at wavenumber $\tilde{\nu}$. [b]TRF technique, monoexponential fit, error: ±10%. [c]Single photon counting, monoexponential fit, error: ±0.1 ns. [d]Second maximum at 25000 cm^{-1} (see Figure 3). [e]T = 93 K. [f]References 56−58.

DOI: 10.1021/jp510856u
J. Phys. Chem. B XXXX, XXX, XXX−XXX

only for the time period in which the opening pulse penetrates the Kerr medium (CS_2). The opening pulse is delayed with respect to the exciting one with an optical delay line (maximum delay of 3000 ps, 0.1 ps/step). The fluorescence is transmitted to the detection system by a quartz fiber. The detection system consists of a polychromator (Action SpectraPro-275) and a CCD detector (Princeton Instruments Inc.). The temporal resolution of the spectrofluorimeter is 6 ps. The spectra were corrected for the instrumental spectral response. Relaxation of the solvent cage is accompanied by TRF spectral shift, which is monitored using an empirical solvation function $c(t)$ defined by $c(t) = [\tilde{\nu}(t) - \tilde{\nu}(\infty)]/[\tilde{\nu}(0) - \tilde{\nu}(\infty)]$; $\tilde{\nu}(0)$, $\tilde{\nu}(t)$, and $\tilde{\nu}(\infty)$ are the fluorescence maxima observed immediately after excitation, at some delay after excitation, and at the time sufficiently long to reach equilibrium, respectively.[32] The $c(t)$ curves were fitted to multiexponential decays.

Ground state geometries were optimized using density functional theory (DFT) with the B3LYP hybrid functional. For vertical excitation energies and excited state geometry optimizations, the time-dependent DFT (TD-DFT) approach was applied. Since the B3LYP functional, due to an incorrect asymptotic behavior ($1/r$), tends to underestimate the energies of electronically excited states with a charge transfer character (CT), sometimes very severely,[33] its long-range-corrected version CAM-B3LYP[34] was employed in the TD-DFT procedure, that in most cases cures B3LYP drawbacks.[35] To double check, the excited state results were recalculated by the configuration interaction singles (CIS) method, which, despite an overall worse description of excitation energies than TD-DFT, gives a more balanced description of local valence and CT states.[33] To obtain different rotational/pyramidalization profiles, respective pairs of dihedral angles were constrained during optimization. Independently, geometries of stationary points were localized by full optimization followed by Hessian matrix calculation. The 6-31G* basis set was used in all calculations. For some of the stationary points, we checked that the extension of the basis set to 6-31+G** did not significantly influence the computational results. All calculations were performed using the Gaussian 09 suite of programs.[36]

3. RESULTS

3.1. Steady-State Spectroscopy. *3.1.1. Room Temperature Absorption and Fluorescence.* Room temperature absorption and fluorescence spectra of ADAB were recorded in a number of aprotic solvents characterized by different polarity indices. The shape and the spectral position of the first absorption band are only weakly dependent on solvent polarity (see Figure 1). Contrary to the absorption, the fluorescence spectra recorded in a liquid phase are strongly solvent-dependent (Figure 1, Table 1). Increasing the polarity of the solvent shifts the wavelength of the emission maximum significantly to the red. No correlation of the room temperature fluorescence maxima with solvent viscosity was observed. The transition dipole moments in emission and absorption do not show dependence on the solvent.

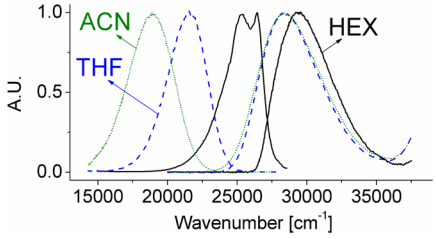

Figure 1. Room temperature absorption and fluorescence spectra of ADAB recorded in HEX, THF, and ACN; excitation energy ($\tilde{\nu}_{exc}$) = 29400 cm^{-1}.

The excited state dipole moment was determined using the relation proposed by Bilot, Kawski, and Liptay[37,38] (eq 1). The quantitative determination of the excited state dipole moment (μ_e) was performed using the linear fit of the fluorescence maxima $\tilde{\nu}_{max}$ versus the polarity functions $F_1(\varepsilon, n^2)$ and $F_2(\varepsilon, n^2)$ according to Lippert−Mataga[39,40] (eq 2) and McRae[41] (eq 3). The values of μ_e were estimated as 25 ± 3 D using eq 2 and 18 ± 2 D using eq 3 (Figure 2).

$$\nu_{max} = \nu_{max}^{vacuum} - \frac{2\mu_e(\mu_e - \mu_g)}{hca_0^3} F(\varepsilon, n^2) \quad (1)$$

where

$$F_1(\varepsilon, n^2) = \frac{\varepsilon - 1}{2\varepsilon + 1} - \frac{1}{2}\frac{n^2 - 1}{2n^2 + 1} \quad (2)$$

$$F_2(\varepsilon, n^2) = \frac{\varepsilon - 1}{\varepsilon + 2} - \frac{1}{2}\frac{n^2 - 1}{n^2 + 2} \quad (3)$$

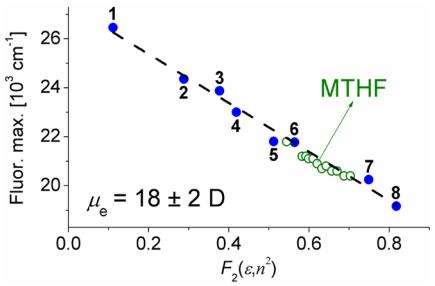

Figure 2. Solvatochromic (full circles) shift of the fluorescence maxima of ADAB in aprotic solvents at room temperature (see Table 1 for solvent numbering) and thermochromic shift (294−133 K) of the fluorescence maxima of ADAB in MTHF (open circles); the data for ε and n were selected from ref 43. The evaluated excited state dipole moment is 18 ± 2 D.

The values of the ground state dipole moment and the Onsager cavity radius were assumed to be equal to 5.65 D and 6 Å, respectively, as for 4-dimethylamino-4′-cyanobiphenyl.[42] The plot of the thermochromic shift of the fluorescence maximum of ADAB in MTHF[43] corresponds well with the solvatochromic plot (Figure 2).

3.1.2. Temperature Dependence of Absorption and Fluorescence. Absorption and emission spectra of ADAB were recorded as a function of temperature in BE, MTHF, and BuCN (Figure 3). In these solvents, the first absorption band exhibits at low temperatures a red shift of the maximum, reflecting some ground state structural changes and/or changes in the population of the ground state vibrational levels.

The maxima of the fluorescence of ADAB recorded in liquid solvents at selected, monotonically decreasing temperatures reveal a red shift (Figure 3). Near the freezing point, a reversed tendency is observed (Figure 4B). It is worth mentioning that at 77 K (rigid solvents) the maximum of emission of ADAB is located almost at the same spectral position independent of the

DOI: 10.1021/jp510856u
J. Phys. Chem. B XXXX, XXX, XXX−XXX

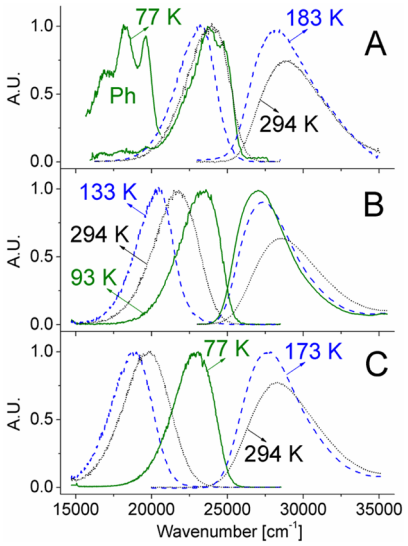

Figure 3. Room and low temperature absorption, fluorescence, and phosphorescence (Ph) spectra of ADAB in BE (A), MTHF (B), and BuCN (C); $\tilde{\nu}_{exc}$ = 29400 cm^{-1}. Fluorescence and phosphorescence are normalized to unity. Absorption is normalized to the low temperature spectrum.

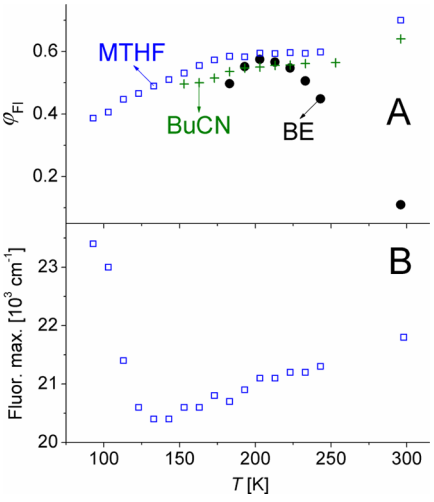

Figure 4. (A) Fluorescence quantum yields (φ_{Fl}) of ADAB measured as a function of temperature in BE, MTHF, and BuCN. (B) Fluorescence maxima of ADAB in MTHF measured as a function of temperature.

solvent polarity (Table 1). The phosphorescence of ADAB is observed only in rigid BE.

The temperature dependences of the quantum yields (QYs) of ADAB measured in solvents of different polarity are presented in Figure 4A. In MTHF and BuCN, the decrease of the temperature leads to a decrease of the QY. Contrary to that, in BE, the QY recorded as the function of the temperature exhibits the maximum at about 203 K.

3.1.3. Model Compound (ADAB-Me). The maximum of the first absorption band of ADAB-Me in *n*-hexane (32200 cm^{-1}) is located at a considerably higher energy than in ADAB (29350 cm^{-1}), see Figure 5. Room temperature fluorescence of ADAB-Me in protic and aprotic solvents was undetectable. Low temperature total luminescence recorded in BuCN consists of phosphorescence (Figure 5). The low temperature total luminescence and phosphorescence excitation spectra are

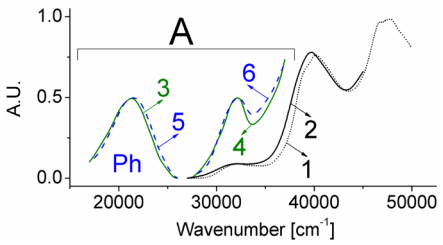

Figure 5. Room-temperature absorption spectra of ADAB-Me in *n*-hexane (1) and BuCN (2). (A) Low temperature (77 K) spectra of ADAB-Me in BuCN: luminescence (3), luminescence excitation (4), phosphorescence (5), phosphorescence excitation (6).

identical, showing the first band in the same spectral region as the room temperature absorption.

3.2. Time-Resolved Experiments. The results of the time-resolved experiments for ADAB in liquid phase are presented in the order of increase of solvent polarity: nonpolar (*n*-hexane), moderately polar (MTHF), and polar (acetonitrile) solvents. In *n*-hexane, the time-resolved fluorescence (TRF) band is observed within the spectral region of 21000−27000 cm^{-1} (Figure 6A). There is no observable spectral evolution of this

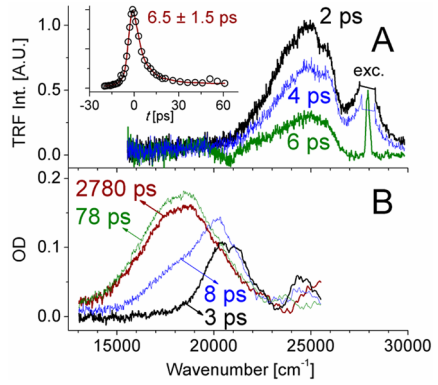

Figure 6. ADAB in *n*-hexane at room temperature. (A) TRF spectra recorded as a function of the delay time (the spectra were not corrected for the apparatus spectral response). Inset, the kinetic curve of the TRF decay, integration limit 22200−25000 cm^{-1}; solid line: monoexponential fit. (B) TA spectra recorded as a function of the delay time.

band. It should be pointed out that fluorescence is located near the excitation line, and therefore, the filters cut out seriously the high-energy part of this spectrum. This is the reason why the TRF spectra recorded in *n*-hexane were not corrected for the spectral response of the apparatus. The decay time (τ) of the fluorescence of ADAB in *n*-hexane is 6.5 ± 1.5 ps (Figure 6A); it is thus only a few picoseconds shorter than the τ recorded in cyclohexane (Table 2).

Transient absorption (TA) spectra recorded for ADAB in *n*-hexane at room temperature are presented in Figure 6B.

For ADAB in *n*-hexane, the kinetics of TA consists of a fast decay or a fast rise depending on the observation wavelength. In both cases, a long decay component is observed. Within the accessible time scale (0−3 ns), this component can be treated as constant (Figure S1, Supporting Information). In order to find its temporal behavior, the decay curves of the transient absorption were recorded in the nano- to microsecond domains. The evaluated decay time is equal to 50 ± 5 ns and shows no dependence on observation wavenumber $\tilde{\nu}_{obs}$ within

DOI: 10.1021/jp510856u
J. Phys. Chem. B XXXX, XXX, XXX−XXX

Table 2. Decay Times (τ) Calculated from TRF Experiments and Decay/Rise Times ($\tau/{}^{R}\tau$) Obtained from TA Experiments for Selected Observation Ranges $\langle\tilde{\nu}_{obs}\rangle$ for ADAB in Nonpolar and Weakly Polar Solvents at 294 K

	TRF		TA			
	τ (ps)	$\langle\tilde{\nu}_{obs}\rangle$ (10^3 cm^{-1})	τ (ps)	$\langle\tilde{\nu}_{obs}\rangle$ (10^3 cm^{-1})	${}^{R}\tau$ (ps)	$\langle\tilde{\nu}_{obs}\rangle$ (10^3 cm^{-1})
n-hexane	6.5 ± 1.5	22.2–26.3	8 ± 1	22.0–22.2	6.5 ± 1.0	15.6–18.5
cyclohexane	9.4 ± 0.7	21.3–25.6	11 ± 1.7	20.6–22.5	10.5 ± 2	15.6–18.5
BE	295 ± 16	21.7–22.7	280 ± 20	20.0–22.2	*a*	

[a]The TA band was not intensive enough to obtain an acceptable kinetic curve.

the long-wavelength band. The decay/rise times obtained from the emission/absorption time-resolved experiments for ADAB in nonpolar solvents are collected in Table 2.

Room temperature TA spectra recorded for ADAB in BE (ε = 3.08) (Figure 7C) and diisopropylether (ε = 3.88) exhibit the same features as the spectra recorded in nonpolar solvents. After excitation, stimulated emission and a short-wavelength TA band are observed. For longer delay times, a new band grows, located within the spectral region of 14500–18200 cm^{-1}. The intensity of this band crucially depends on solvent polarity: in more polar diethyl ether, the long-wavelength band is not observed.

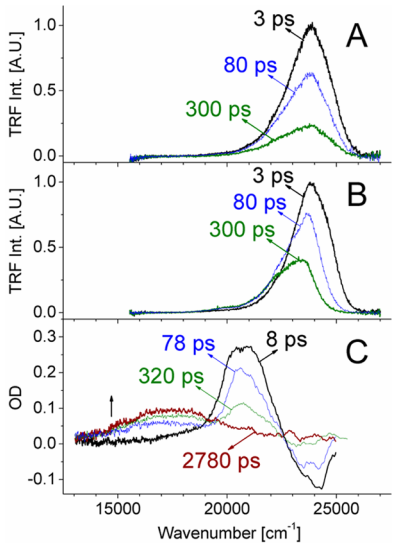

Figure 7. ADAB in BE, TRF spectra recorded as a function of the delay time at 294 K (A) and 203 K (B). Room temperature TA spectra recorded as a function of the delay time (C).

Room temperature TRF spectra of ADAB in BE show maxima at 24000 cm^{-1} independent of the delay time (Figure 7A); however, it should be stressed that just after excitation the blue edge of the spectrum undergoes a small red shift. At low temperature, the temporal evolution of TRF spectra is observed (Figure 7B). The character of the kinetic curves depends strongly on the observation wavelength. The blue part of the TRF spectra reveals a non-monoexponential decay, whereas the kinetic curves obtained by integration of the long-wavelength part of the TRF exhibit a rise and slow decay. The calculated values of the decay/rise times are collected in Table S1 (Supporting Information).

The TRF spectra of ADAB in MTHF (ε = 7) at 294 K are presented in Figure 8A. The TRF spectra show negligible dependence on the delay time. At intermediate temperatures (133 K, Figure 8B), the TRF spectrum is composed of two bands. Just after excitation, the maximum of the high energy band is located at about 23500 cm^{-1}. During the next 50 ps, this band decays and, simultaneously, its maximum shifts by 2000 cm^{-1} to the red. At 100 ps after excitation, the spectrum is dominated by the low energy band. This band exhibits a negligible time-dependent shift. For ADAB at 93 K (Figure 8C), only the high energy band is observed and the spectral evolution of the TRF spectra is not detectable.

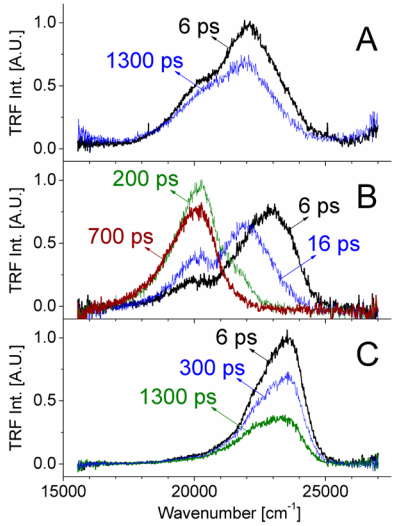

Figure 8. TRF spectra of ADAB in MTHF recorded as a function of the delay time at 294 K (A), 133 K (B), and 93 K (C).

A typical spectral-solvent response function, $c(t)$, obtained for the fluorescence maximum of the short-wavelength band is presented in Figure S2 (Supporting Information). The relaxation times (τ_s) evaluated from the $c(t)$ functions at selected temperatures are collected in Table 3. This table also contains the literature values used to characterize the relaxation of MTHF.

On the basis of experimental observations, the decay times of the fluorescence of ADAB in MTHF calculated from the kinetic curves obtained for the number of $\tilde{\nu}_{obs}$ at various temperatures (Table S2, Supporting Information) can be categorized as follows:

(i) The blue part of the emission (22200–25000 cm^{-1}) exhibits mono- or biexponential decays. The decay time corresponding to the fast component increases for decreasing $\tilde{\nu}_{obs}$ (observation range).

(ii) The red part of the emission exhibits the rise and decay; the rise time depends on the $\tilde{\nu}_{obs}$ in the same way as the decay time of the fast component.

For ADAB in MTHF, the experimental points of the $\ln(\tau)$ vs $1/T$ obtained for two $\langle\tilde{\nu}_{obs}\rangle$ are presented in Figure S3 (Supporting Information). The average value of the activation energy calculated from the slopes of the linear fits is equal to 510 ± 50 cm^{-1}.

DOI: 10.1021/jp510856u
J. Phys. Chem. B XXXX, XXX, XXX–XXX

Table 3. Relaxation Times (τ_s) Calculated from $c(t)$ Plots for ADAB in MTHF Compared with the Relaxation Times of MTHF Obtained by Maroncelli and His Co-Workers for 4-Aminophthalimide (4-AP) as a Probe[59] or by the Dielectric Loss Measurements[60]

ADAB/MTHF		4-AP/MTHF		MTHF
T (K)	τ_s (ps)	τ_{s1} (ps)	τ_{s2} (ns)	τ_s[d] (ps)
173	<6	52[a]	0.14[a]	
153	9 ± 2	73[b]	0.42[b]	40
133	29 ± 3	307[b]	3.4[b]	200
123	94 ± 13	810[b]	6.2[b]	1000
113	177 ± 13			100000
103	875 ± 100		7 × 10[6 c]	

[a] T = 170 K. [b] Values obtained by interpolation. [c] Quinoxaline was used as the probe (T = 96 K). [d] Data evaluated from the plot in Figure 1 in ref 59.

The room temperature TRF spectra of ADAB in the nitriles BuCN (ε = 20.3) and ACN (ε = 37.5) are presented in Figures 9 and 10, respectively. In BuCN, just after excitation, a shoulder

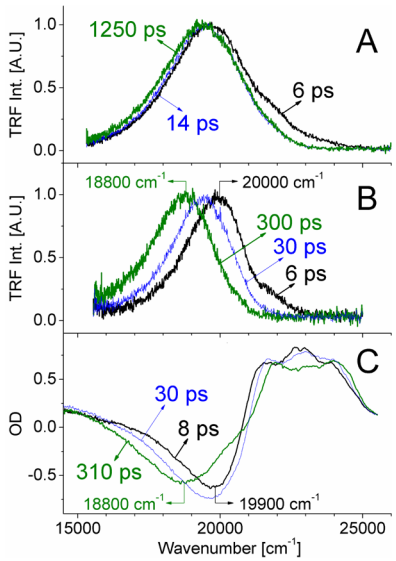

Figure 9. ADAB in BuCN, normalized TRF spectra recorded as a function of the delay time at 294 K (A) and 173 K (B). TA spectra recorded as a function of delay time at 173 K (C).

located at the blue side of the main band is observed, whereas, in more polar ACN, this shoulder is undetectable. For both solvents, the maximum of the main band remains almost the same for short and long delays; its spectral position depends on solvent polarity: 19600 cm^{-1} (BuCN), 18900 cm^{-1} (ACN). The TA spectra of ADAB in ACN consist of the absorption bands located within the spectral regions 21300−25000 and 13000−16000 cm^{-1} and stimulated emission with the maximum at 18800 cm^{-1}. The latter value corresponds well to the maximum of the TRF. The spectral distribution of the TA spectra does not depend on the delay time.

TRF spectra of ADAB recorded just after excitation in BuCN at 173 K exhibit a shoulder located at the blue side of the main band ($\tilde{\nu}_{max}$ = 19900 cm^{-1}). The maximum of this band shows a time-dependent red shift (Figure 9B). TA spectra of ADAB in BuCN recorded at 173 K consist of the absorption band (21500−25000 cm^{-1}) and stimulated emission (16000−21500

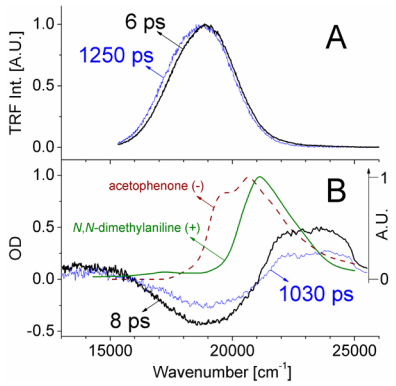

Figure 10. ADAB in ACN at 294 K. (A) Normalized TRF spectra recorded as a function of the delay time. (B) TA spectra recorded as a function of the delay time and compared with the spectra of anion and cation radicals of acetophenone and *N,N*-dimethylaniline, respectively.

cm^{-1}). The time-dependent shift of the maximum of the stimulated emission is easily observed (Figure 9C). The relaxation times evaluated from both TRF and TA are collected in Table 4.

3.3. Calculations. *3.3.1. Cross Sections along the Θ Coordinate.* To investigate the nature of the electronic states of ADAB upon twisting of the acetophenone group with respect to the *N,N*-dimethylaniline moiety, ground state DFT and excited state TD-DFT (Figure 11) and CIS (Figure S4, Supporting Information) quantum chemical calculations were performed for different values of the dihedral angle Θ. Except for specific cases, we provide below the numerical values for excited states obtained using TD-DFT, which are considered more reliable. The potential is not symmetric with respect to Θ = 0° (and in most cases for Θ = 90°) when either the *N,N*-dimethylaniline (S_0 and $^1n\pi^*$ states) or the acetophenone ($^1n\pi^*$ state) group is not planar. The differences in energies of all considered electronic states between possible conformers are, however, not significant (lower than 0.2 kcal/mol) and hereafter the results will be analyzed in a reduced Θ range of 0−90°.

The results of the calculations indicate that the most stable ground state conformation is obtained when the acetophenone moiety is twisted with respect to the *N,N*-dimethylaniline (DMA) by Θ = 34°. The barriers to rotation are not high, especially that corresponding to Θ = 0° (1.4 vs 3.2 kcal/mol for 90°). The dipole moment value changes with Θ only slightly, within the range 5.0−6.4 D, being higher for lower twist angles. The dimethylamino group in S_0 is pyramidalized by δ = 9°; the acetophenone unit is planar.

The relative position of two lowest excited singlet states which are of the $^1n\pi^*$ and $^1\pi\pi^*$ (L_a) type crucially depends on the Θ angle and also on whether the ground or excited state is optimized. The computed energy and the dipole moment values of the $^1n\pi^*$ state do not show significant dependence on the Θ angle (Figure 11 and Figure S4, Supporting Information). The shape of the $^1n\pi^*$ potential strongly resembles that of S_0. The energy minimum is observed at 34°, and the dipole moment for all values of the Θ angle is about 2−3 D. The *N,N*-dimethylamino group gets more pyramidalized (δ = 11°), and the acetylo unit goes slightly out of planarity (ω = 3°) after $^1n\pi^* \leftarrow S_0$ excitation. As expected, the oscillator strength for $^1n\pi^* \leftarrow S_0$ transitions is very low (<0.003). Contrary to the situation in the S_0 and $^1n\pi^*$ states,

DOI: 10.1021/jp510856u
J. Phys. Chem. B XXXX, XXX, XXX−XXX

Table 4. Relaxation Times (τ_s) Evaluated from the $c(t)$ Function Determined from the Spectral Position of the TRF and Stimulated Emission (TA) Maxima for ADAB in BuCN at Low Temperatures, Compared with the Literature Data Obtained Using Optical Kerr Effect Spectroscopy[61] and the Spectral Response Function of the 4-Dimethylamino-4′-cyanostilbene (DCS) Probe Molecule[62]

ADAB/BuCN		BuCN/Kerr				DCS/BuCN			
T (K)	τ_s (ps)	τ_{s1} (ps)	τ_{s2} (ps)	$\langle\tau_s\rangle^a$ (ps)	A_1, $A_2{}^a$	τ_{s1} (ps)	τ_{s2} (ps)	$\langle\tau_s\rangle^a$ (ps)	A_1, $A_2{}^a$
203	26 ± 2^{TA}, 24 ± 3^{TRF}	7.2	27.1	23.3	0.19, 0.81	9	41	12.8	0.88, 0.12
173	92 ± 5^{TA}, 83 ± 5^{TRF}	21	95	83.2	0.16, 0.84	20	138	60.1	0.66, 0.34
163	153 ± 10^{TRF}	30[b]	145[b]	126.6	0.16, 0.84	26	237	142	0.45, 0.55

[a] $\langle\tau_s\rangle = A_1\tau_{s1} + A_2\tau_{s2}$, where A_1 and A_2 are τ_s-corresponding amplitudes. [b] Extrapolation of the data.

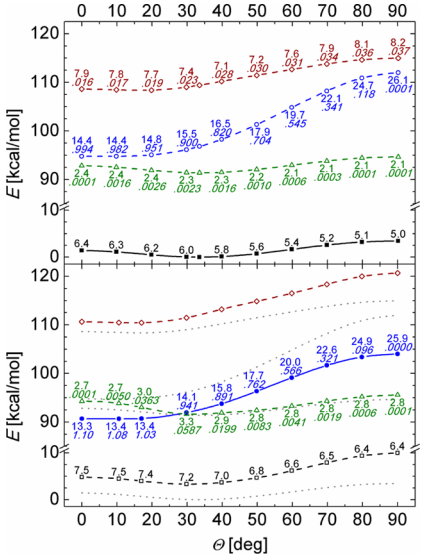

Figure 11. Scheme of the energy levels of ADAB calculated (TD-DFT) as a function of the twist angle Θ for the ground (upper panel) and excited $^1\pi\pi^*$ (CT) (lower panel) state, DFT and TD-DFT optimized geometries, respectively. Squares, S_0; triangles, $^1n\pi^*$; circles, $^1\pi\pi^*$ (CT); diamonds, $^1\pi\pi^*$ (L_b). Full symbols and solid lines correspond to the optimized states. The upper numbers indicate the values of the dipole moment (D), the lower ones, S_n–S_0 oscillator strengths.

the energy of the lowest $^1\pi\pi^*$ state significantly decreases upon flattening of ADAB, reaching the minimum at a value of Θ close to 0°. The $^1\pi\pi^*$ state optimization yields a structure with Θ = 11°; however, a flat system has almost the same energy (using CIS, a totally planar structure is obtained). Also, in contrast to the S_0 and $^1n\pi^*$ states, the *N*,*N*-dimethylaniline group becomes planar after $^1\pi\pi^* \leftarrow S_0$ excitation in the whole Θ range. For the ground state geometry, the computed $^1\pi\pi^*$ excited state energy stabilization due to planarization (from Θ = 34 to 0°) is 700 cm^{-1}. A much more significant stabilization takes place when the $^1\pi\pi^*$ excited state geometry transformation occurring along the relaxation path is taken into account. It equals 2200 cm^{-1}, when the starting and ending points are described by the ground and excited state geometries, respectively. The dipole moment of the $^1\pi\pi^*$ is substantially higher than that in S_0 and increases monotonically starting from 13.3 D (Θ = 0°) up to 25.9 D (Θ = 90°), see Figure 11. Thus, the lowest $^1\pi\pi^*$ (L_a) ← S_0 transition in our system has a significant charge transfer (CT) character. The oscillator strength, large for small Θ values, decreases upon twisting. These trends are consistent with the results obtained by Maus et al.[42] for a cyano analogue of ADAB. For fully twisted subgroups of ADAB (Θ = 90°), a large dipole moment (25.9 D) and a small value of the oscillator strength (<10^{-4}) of the $^1\pi\pi^*$ (CT) state suggest that this state can be assigned to TICT.[19] However, its energy is destabilized by 4700 cm^{-1} with respect to the energy of the $^1\pi\pi^*$ (CT) state of the planar conformer. The energy of the higher $^1\pi\pi^*$ (L_b) singlet state does not depend so drastically on Θ (Figure 11), and so does the dipole moment value (7–8 D). The oscillator strength for the $^1\pi\pi^*$ (L_b) ← S_0 transition is low (0.016–0.037) and increases with Θ.

The molecular orbitals involved in the three above-mentioned low-lying electronic transitions in ADAB calculated for selected Θ angles are presented in Figure 12. The low-energy $^1\pi\pi^*$ (CT) ← S_0 transition can be approximated by a HOMO–LUMO configuration (>85%). The shapes of the orbitals depend on Θ. For the planar geometry (Θ = 0°), the HOMO and LUMO are spread over the whole molecular

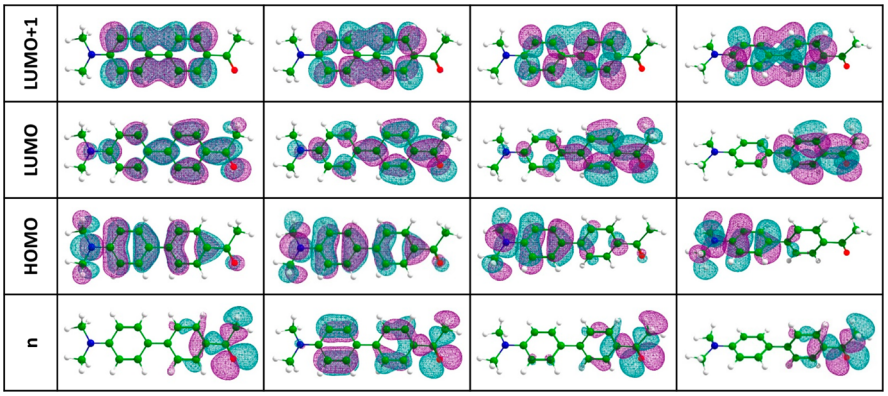

Figure 12. Molecular orbitals of ADAB involved in $^1n\pi^* \leftarrow S_0$ (n-LUMO), $^1\pi\pi^*$ (CT) ← S_0 (HOMO–LUMO), and $^1\pi\pi^*$ (L_b) ← S_0 (HOMO–LUMO+1) transitions, calculated for Θ = 0, 30, 60, and 90°.

DOI: 10.1021/jp510856u
J. Phys. Chem. B XXXX, XXX, XXX–XXX

skeleton; nonetheless, they are more concentrated on the donor and acceptor units, respectively. The increase of Θ generates a further localization of these orbitals, and consequently, for a twisted geometry (Θ = 90°), the HOMO is associated exclusively with the donor, whereas the LUMO with the acceptor subunit. The n orbital involved in the $^1n\pi^* \leftarrow S_0$ transition (n-LUMO) is localized mainly on the acetophenone subunit. The $^1\pi\pi^*$ (L_b) $\leftarrow S_0$ excitation is well described by a HOMO−LUMO+1 configuration. The LUMO +1 orbital is spread over the full biphenyl skeleton, independent of the twist angle. The polarization of this transition, perpendicular to the long axis of the system, validates its L_b-type description.

The properties of the three lowest excited singlet states obtained by the CIS method (Figure S4, Supporting Information) in general agree with the TD-DFT results. The most significant difference is in the Θ dependence of the $^1\pi\pi^*$ (CT) energy profile, which is much more steep according to CIS. The destabilization energy of this state due to twisting, obtained for the ground state geometry, reaches 15100 cm^{-1} and is 2.5 times more than the TD-DFT value (6000 cm^{-1}). As a consequence, the $^1\pi\pi^*$ (CT) state is no longer the lowest $^1\pi\pi^*$ state for high values of Θ (>60°) and has to be correlated with one of the higher excited states (Figure S4, Supporting Information). We also failed to optimize $^1\pi\pi^*$ (CT) in that Θ range. The CIS method predicts smaller dipole moment values of the $^1\pi\pi^*$ (CT) state than TD-DFT. At this stage, it is not possible to decide which picture is more realistic. On one hand, the long-range corrected CAM-B3LYP functional may still not be ideal for all TICT systems; on the other, CIS, as a simple noncorrelated approach, is also known to have problems with strongly polar excitations (e.g., it fails to localize the energy minimum at 90° for the TICT structure in DMABN). More advanced, multireference computations are mandatory.

It was verified using ground state geometry and CIS as well as TD-DFT models that reasonable structural changes, such as rotation of the dimethylamino or aldehyde groups and pyramidalization of the former, do not generate multiple minima on the potential energy surfaces of the analyzed lowest excited states of ADAB (Figures S5−S7, Supporting Information).

Boltzmann distributions of differently twisted ADAB molecules calculated as a function of Θ in S_0 and $^1\pi\pi^*$ (CT) states are presented in Figure S8 (Supporting Information). It should be noticed that at room temperature the ground state Boltzmann distribution spreads from 10° up to 55° (90% of population, 70% for 20° to 45°). The polar environment shifts it to the lower Θ values.

The results of DFT/TD-DFT calculations performed for ADAB-Me (Figure 13) give, in principle, a similar picture to that of ADAB, but after adding substantial barriers for angles Θ = 0 and 180° (about 15 and 25 kcal/mol, respectively) to all electronic states resulting from steric hindrance imposed by methyl substitution in both phenyl rings. As a consequence, the most stable ground state conformation is obtained when the acetophenone moiety is twisted with respect to the *N,N*-dimethylaniline by almost 90° (84, 94, 92, and 77° for four almost isoenergetic isomers, differing in relative conformations of the dimethylamino or aldehyde groups with respect to the methyl substituents in phenyl rings). Similarly, as in the case of ADAB, the energy profile for the $^1n\pi^*$ state of ADAB-Me follows strictly that of S_0 and its dipole moment does not depend on Θ. The energy of the lowest $^1\pi\pi^*$ (CT) state

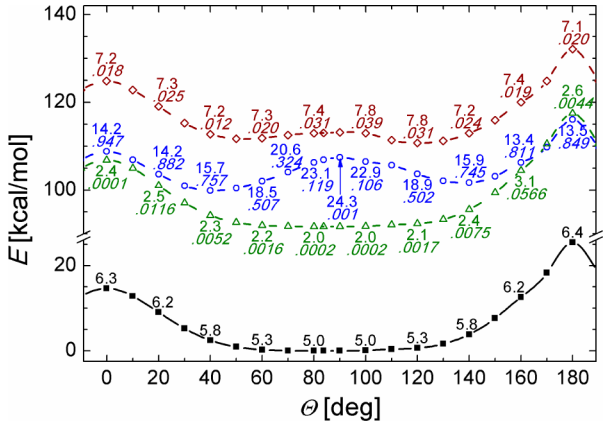

Figure 13. Scheme of the energy levels of ADAB-Me calculated using TD-DFT as a function of the twist angle Θ for the ground state optimized geometry. See Figure 12 for details.

strongly decreases upon flattening of ADAB-Me, but due to methyl hindrance, it reaches a minimum around 40° (47° after optimization). As a consequence, the $^1n\pi^*$ remains the lowest excited state even at the $^1\pi\pi^*$ state optimized geometry. The dipole moment value and the oscillator strength of the $^1\pi\pi^*$ (CT) state strongly increase and decrease with Θ, respectively, reaching 24.3 D and 0.001 for a fully twisted system.

3.3.2. Comparison of the Results of Calculations with the Experimental Data. The comparison between the experimental transition energies and the corresponding calculated values is given in Table 5.

The calculated vertical $S_n \leftarrow S_0$ excitation energies are evidently higher than the experimental values derived from absorption spectra in nonpolar solvents. It is well-known that the CIS model significantly overestimates the energy of the excited states. The TD-DFT model predicts that the $^1\pi\pi^*$ (CT) state (33900 cm^{-1}) lies about 1900 cm^{-1} higher on the energy scale than $^1n\pi^*$ (32000 cm^{-1}), whereas the CIS calculations predict both states to be almost isoenergetic (39900 and 40300 cm^{-1}, respectively). The maximum of the first absorption band of ADAB in *n*-hexane is located at 29400 cm^{-1} (Figure 1). Due to the overlap of weak $^1n\pi^*$ and strong $^1\pi\pi^*$ bands, the spectral position of the maximum of the $^1n\pi^*$ band is unknown. According to the results of calculations, the orbitals involved in the $^1n\pi^* \leftarrow S_0$ transition are mainly localized on the acetophenone subunit; consequently, the energy of the $^1n\pi^*$ state of ADAB should be well approximated by the energy of the *para*-substituted derivatives of acetophenone. For 4-(dimethylamino)acetophenone, 4-hydroxyacetophenone, and 4-methoxyacetophenone, the corresponding energies of the lowest singlet states of nπ^* character were established at 28500,[13] 28900,[44] and 28400 cm^{-1},[44] respectively. It should be pointed out that the confrontation of the calculated energy of the transitions with the absorption maxima in the case of the ADAB molecule can generate some doubts, because, at room temperature, the ground state Boltzmann distribution, calculated as the function of Θ (Figure S8, Supporting Information), spreads from 10 to 55°. The energy and probability of the transition depend on Θ. Therefore, one should be careful regarding the accuracy of calculations, especially with respect to the sequence of the two low-lying $^1n\pi^*$ and $^1\pi\pi^*$ states. However, it is worth noting that enlarging the basis set to 6-31+G** decreases the energy of the $^1\pi\pi^* \leftarrow S_0$ transition by 1000 cm^{-1} while leaving the $^1n\pi^* \leftarrow S_0$

DOI: 10.1021/jp510856u
J. Phys. Chem. B XXXX, XXX, XXX−XXX

Table 5. Results of the TD-DFT and CIS/6-31G* Calculations (E, $S_n \leftarrow S_0$ Vertical Excitation Energy; μ, S_n Dipole Moment; 6-31+G** Values in Brackets), Performed for the Ground State Geometry ($\Theta = 34°$) Compared with the Experimental Data

	calculations					
	TD-DFT		CIS		experimental data	
S_n	E (cm^{-1})	μ (D)	E (cm^{-1})	μ (D)	E (cm^{-1})	μ (D)
$^1n\pi^*$	32000 (31900)	2.3 (2.6)	39900 (40000)	2.7 (2.6)	28500[a]	
$^1\pi\pi^*$ (CT)	33900 (32900)	15.8 (16.4)	40300 (39100)	9.9 (10.4)	29350[b]	18 ± 3[e]
$^1\pi\pi^*$ (L_b)	38300 (36800)	7.3 (7.6)	45500 (43600)	6.5 (6.6)	32800[c]	
$^1\pi\pi^*$ (DMA)	47400		58400		41700[d]	

[a]Maximum of the absorption band ($^1n\pi^* \leftarrow S_0$) for 4-(dimethylamino)acetophenone; see ref 13. [b]Maximum of the first absorption band of ADAB in *n*-hexane; from the absorption/fluorescence intersection, a value of 27200 cm^{-1} was obtained. [c]MCD experiment performed for ADAB in THF; see Figure S10 (Supporting Information). [d]Maximum of the second absorption band for ADAB in *n*-hexane. [e]Derived from a solvatochromic plot for emission.

energy almost intact (at 31900 cm^{-1}). As a result, very good agreement between computations and experiment is found for the relative position of the two low-lying excited states (see Table 5). Also, the $^1\pi\pi^*$ (CT)−$^1\pi\pi^*$ (L_b) separation inferred from the MCD spectrum is well reproduced.

We now compare the results of quantum chemical calculations and the experimental data for emission. As was described before, the ordering of the $^1n\pi^*$ and $^1\pi\pi^*$ states depends on the excited state geometry (Figure 11). The high values of the radiative rate constant and transition dipole moment (Table 1) indicate that the emission originates from the $^1\pi\pi^*$ state. For the $^1\pi\pi^*$ optimized geometry, the computed energy of the $^1\pi\pi^* \rightarrow S_0$ (CT) transition is 29800 cm^{-1}; the $^1n\pi^*$ state is located 1100 cm^{-1} higher. The maximum of fluorescence of ADAB in *n*-hexane is observed at 26450 cm^{-1}. The energy of the $^1\pi\pi^*$ (CT) state evaluated from the absorption/fluorescence intersection is equal to 27200 cm^{-1}. The dipole moment deduced from the plot of the solvatochromic shift is 25 ± 3 D (eq 2) or 18 ± 3 D (eq 3). Having in mind the excited state relaxation along the Θ angle, contributing to the solvatochromic shift, this last value corresponds acceptably to 13.4 D, the value calculated for the $^1\pi\pi^*$ state. The results of TD-DFT calculations reproduce significantly better the experimental data than the results obtained using CIS.

4. DISCUSSION

The Stokes shift of ADAB emission strongly depends on the solvent polarity; however the transition moment in emission is approximately constant and equal to the transition moment in absorption, which suggests that, independently of environment, the emitting state is of $^1\pi\pi^*$ type, as in the case of the cyano[42] and pyridine[45] analogues of ADAB. The radiative rates (k_f) decrease in polar solvents (Table 1), probably due to the lower transition energy. A similar effect was reported for 4-formyl-4′-(dimethylamino)biphenyl and attributed to interaction with a higher-lying singlet state having a large dipole moment and small radiative transition probability.[46] The radiationless depopulation rate depends on the polarity of the environment (Table 1), which will be discussed later. At room temperature, the maximum of the stationary emission as well as radiative and nonradiative rate constants do not exhibit a correlation with solvent viscosity (Table 1).

The results of quantum chemical calculations indicate that the most stable ground state conformation is for the acetophenone subgroup twisted with respect to the dimethylanilino moiety by $\Theta = 34°$. The same value of Θ was evaluated from the crystallographic data.[28]

After excitation, the angle Θ can increase or decrease its value. The first case corresponds to a relaxation to the TICT state, when the dimethylaniline and acetophenone subgroups are mutually twisted around the central bond by 90°. In the second case, after excitation, ADAB reaches a more planar structure than in the ground state.

4.1. Possible Relaxation Path: S_1 (Primary Excited) → TICT → S_0. The model compound ADAB-Me, with the aromatic rings mutually pretwisted ($\Theta \approx 90°$), does not emit fluorescence in polar solvents at room temperature. The low temperature luminescence was assigned as phosphorescence, indicating a fast singlet−triplet depopulation channel. The absence of TICT emission for ADAB-Me can be explained by a rapid intersystem crossing (ISC) to the triplet state.

For ADAB, the dipole moment evaluated from the plot of the solvatochromic shift of the fluorescence maxima is equal to 25 or 18 D depending on the solvatochromic function (eqs 2 and 3), which indicates a CT transfer nature of the lowest excited singlet state. The TICT state can be approximated by the radical anion−cation pair,[12] and consequently, the transient absorption spectra recorded in a polar solvent should be reproduced by the absorption spectra of the corresponding radical pair: *N*,*N*-dimethylaniline (+) and acetophenone (−).[47] It is not the case (cf. Figure 10). High values of the radiative rate constants (Table 1) indicate that the transition is fully allowed, whereas in the TICT model the transition $S_{TICT} \rightarrow S_0$ is forbidden.

The results of quantum chemical calculations show that the energy and the value of the dipole moment of the lowest $^1\pi\pi^*$ (CT) state increase upon twisting and, simultaneously, the oscillator strength decreases (Figure 11). Consequently, the $^1\pi\pi^*$ (CT) state for $\Theta = 90°$ due to high dipole moment (26 D) and small oscillator strength ($<10^{-4}$) can be assigned as the TICT state. This state is predicted to lie 4700 cm^{-1} higher than the computed energy of the $^1\pi\pi^*$ (CT) state for the coplanar arrangement of the *N*,*N*-dimethylaniline and acetophenone groups (Figure 11).

We now analyze the experimental material in terms of the flattening of the ADAB molecule in the excited state.

4.2. Possible Relaxation Path: S_1 (Primary Excited) → S_1 (Semiplanar Geometry) → S_0. *4.2.1. ADAB in n-Hexane and BE.* The room temperature stationary fluorescence band of ADAB in *n*-hexane is observed within the spectral region 21000−28000 cm^{-1} (Figure 1). We found that low temperature luminescence is dominated by the fluorescence of aggregates

DOI: 10.1021/jp510856u
J. Phys. Chem. B XXXX, XXX, XXX−XXX

(15000−22000 cm^{-1}), similarly as in the case of 4-(dimethylamino)benzaldehyde.[47] This is the reason why the phosphorescence of monomers is not observed. However, the phosphorescence of ADAB is detected in slightly more polar BE (Figure 3A). The vibrational structure of the phosphorescence emitted by ADAB in BE reproduces well the vibrational pattern of biphenyl.[48]

The TRF spectrum of ADAB in *n*-hexane is observed within the spectral region 22200−27000 cm^{-1}, and its lifetime is 6.3 ps (see Figure 6A and Table 2). The TA spectrum consists of two bands showing the maxima at 21500 and 18200 cm^{-1} (Figure 6B). Just after excitation, only the short-wave band is observed. The temporal evolution of two TA bands indicates the parent−daughter relation between them. Indeed, the decay time of the primary band is 8 ± 1 ps and the rise of the secondary one is 6.5 ± 1 ps (Table 2 and Figure S1, Supporting Information). The final state is long-lived (50 ns), so it is reasonable to assign the low-energy TA band as the $T_n \leftarrow T_1$ transition and the high-energy one as the $S_n \leftarrow S_1$ transition. The low-energy band is observed in nonpolar and weakly polar solvents: dibutyl (Figure 7C) and diisopropyl ether. In more polar EE, the $T_n \leftarrow T_1$ band disappears. The dependence of the TA spectrum of ADAB on solvent polarity can be directly connected with the sequence of two low-lying states, $^1\pi\pi^*$ and $^3n\pi^*$. The $^1\pi\pi^*$ singlet of ADAB in *n*-hexane is located at 27200 cm^{-1} (intersection of the absorption and fluorescence, Figure 1). The maximum of the $^3n\pi^* \leftarrow S_0$ band for 4-hydroxy- and 4-methoxyacetophenone is located at 27800 and 27400 cm^{-1}, respectively.[44] Consequently, for ADAB in nonpolar solvents, the lowest singlet state is of $^1\pi\pi^*$ type and the $^3n\pi^*$ triplet is almost isoenergetic. Such a configuration of the excited states favors a fast ISC process.[49]

The analysis of the stationary spectra recorded for ADAB in BE gives some additional information concerning the energy dissipation. The room temperature stationary fluorescence spectrum of ADAB recorded in EE shows a 900 cm^{-1} red shift of the maximum in comparison with that recorded in BE. However, the emission recorded in BE at 203 K well matches the fluorescence recorded at 294 K in EE (Figure S9, Supporting Information). This experimental fact indicates that the polarity of BE at 207 K is similar to the polarity of EE at 294 K. The quantum yield and fluorescence decay time obtained for ADAB in BE at 203 K are $\varphi_{Fl} = 0.56$ (Figure 4) and $\tau = 1.7$ ns (Table S1, Supporting Information). The evaluated radiative (k_f) and nonradiative (k_n) rates are 0.35×10^9 and 0.28×10^9 s^{-1}, respectively. The k_f value is independent of temperature, whereas k_n is more than 1 order lower than that evaluated at 294 K and corresponds well to that obtained in EE (Table 1).

The experimental facts presented above indicate that the ISC rate depends on the polarity of the solvent. For ADAB in nonpolar solvents, the following path of the energy degradation can be proposed: $^1\pi\pi^* \rightarrow {}^3n\pi^* \rightarrow {}^3\pi\pi^* \rightarrow S_0$. The inversion of the ordering of $^1\pi\pi^*$ and $^3n\pi^*$ levels favors $^1\pi\pi^* \rightarrow S_0$ relaxation. This inversion takes place for solvents characterized by a dielectric constant of $\varepsilon \approx 4$.

Room temperature solvation dynamics of BE, detected by monitoring the time-dependent Stokes shift of the emission of Coumarin 153, has been studied by Ernsting and Kovalenko.[50] Fitting the solvation response function $c(t)$, they have obtained the following relaxation times: 0.4 ps (0.27), 6.9 ps (0.45), 37.3 ps (0.28) (corresponding amplitudes in brackets). Surprisingly, for ADAB in BE at 294 K, the time-dependent shift of the TRF maximum was not detected. The ground state, room temperature Boltzmann distribution of differently twisted ADAB molecules calculated as a function of the Θ angle spreads from 10 to 55°. The values of the excited state dipole moments vary from 13.3 D for $\Theta = 0°$ to almost 20 D for $\Theta = \pm 60°$ (Figure 11). In this case, the excited state geometry transformation can interact with the solvent cage reorganization, which can hinder observation of the time-dependent shift of the TRF maxima. Indeed, the kinetic curve obtained for the blue edge of the TRF spectrum can be properly approximated by a biexponential decay, whereas for the red tail the rise component is observed (Table S1, Supporting Information). The rise and decay times are equal within the error limit, which indicates the temporal evolution of the fluorescence spectrum. The temporal evolution of the TRF is easily observed at 203 K (Figure 7B and Table S1, Supporting Information). The time constant (monoexponential fit) evaluated from the solvation response function is 220 ± 20 ps.

The ISC transition is a function of the relative position of the polar $^1\pi\pi^*$ with respect to the less polar $^3n\pi^*$ states; the energy gap between them depends on the reorganization of the solvent cage described by the solvent relaxation time. In other words, for ADAB in BE, just after excitation, the k_{ISC} is a function of time.

4.2.2. ADAB in MTHF. The steady state fluorescence of ADAB in MTHF recorded as a function of temperature shows a complex spectral shift. Red shift of the emission is observed within the temperature range 294−133 K, whereas for temperatures lower than 133 K a blue shift is detected (Figures 3B and 4). It should be pointed out that the thermochromic plot down to 133 K and the solvatochromic plot show the same slope, which indicates that low temperature stationary fluorescence of ADAB in MTHF is emitted, except for the time interval just after excitation, from the equilibrated solute−solvent systems (Figure 2). The red shift of the low temperature emission spectra of ADAB in MTHF was successfully correlated with the increase of the solvent polarity.

TRF spectra recorded for selected delay times at 294, 133, and 93 K are presented in Figure 8. Room temperature TRF shows insignificant temporal evolution of the spectral distribution. The TRF recorded at 133 K consists of two bands. The decay of the high-energy band is accompanied by its simultaneous time-dependent spectral shift from $\tilde{\nu}_{max}$ = 23300 cm^{-1} (6 ps) to $\tilde{\nu}_{max}$ = 22000 cm^{-1} (30 ps). Contrary to that, the low-energy band (20200 cm^{-1}) shows a significantly smaller effect of the spectral transformation (Figure 8). In rigid MTHF, the temporal evolution of the emission was not observed. The τ_s values evaluated from the $c(t)$ functions obtained for the high energy band at several temperatures are significantly shorter than the corresponding relaxation times of MTHF (Table 3). A similar effect has been observed for 4-dimethylamino-4′-cyanobiphenyl at 293 K in viscous glycerol triacetate, where the time constant of the charge separation associated with geometry transformation, equal to 67 ps, was evidently faster than the solvent relaxation (≈150 and 690 ps).[51]

4.2.3. ADAB in BuCN. Low temperature TRF spectra of ADAB in BuCN (Figure 9B) consist of the low-energy band. The high-energy band is observed just after excitation as the shoulder on the blue edge of the low-energy band. Contrary to the results obtained in MTHF, the low-energy band reveals a readily detected time-dependent shift. The relaxation times evaluated from the $c(t)$ function determined from the TRF

DOI: 10.1021/jp510856u
J. Phys. Chem. B XXXX, XXX, XXX−XXX

maxima correspond well to those obtained from the shift of the stimulated emission (Table 4).

The low temperature solvation dynamics of BuCN is described by two relaxation times τ_{s1}, τ_{s2} [47, 48]. The τ_s values obtained for ADAB in BuCN at selected temperatures are equal within experimental error to the τ_{s2} values obtained for BuCN by optical Kerr effect spectroscopy (Table 4). The agreement with the relaxation times evaluated from the spectral response function of the probe molecule is worse, suggesting that the local environment reorganization depends not only on the solvent and its temperature but also on the probe molecule.

4.2.4. Solvent-Dependent Excited State Relaxation Path. Both experiment and quantum chemical calculations suggest that two low-lying singlet states can be assigned as $^1n\pi^*$ and $^1\pi\pi^*$ (CT); the third ($^1\pi\pi^*$ (L_b)) is calculated 4400 cm^{-1} (3900 cm^{-1} when 6-31+G** the basis set is applied) higher. This prediction is nicely corroborated by MCD spectra, that reveal the presence of two bands separated by about 3500 cm^{-1} (Figure S10, Supporting Information). Within the accuracy of our calculations, the order of $^1\pi\pi^*$ (CT) and $^1n\pi^*$ states depends critically on the geometry (Figure 11 and Figure S4, Supporting Information) and cannot be unequivocally established. Due to the overlap between two stationary absorption bands which correspond to the $^1n\pi^* \leftarrow S_0$ and $^1\pi\pi^* \leftarrow S_0$ transitions, it is impossible to extract a small $^1n\pi^*$ contribution (Table 5). Consequently, the transition moment in absorption should be characteristic for the $^1\pi\pi^*$ (CT) $\leftarrow S_0$ transition. When internal conversion $^1n\pi^*(\Theta) \rightarrow {}^1\pi\pi^*(\Theta)$ is fast compared with the lifetime, the emission should originate from the $^1\pi\pi^*$ (CT) state, and therefore, transition moments in absorption and emission can be equal, even though the ordering of the states can depend on Θ (Figure 11) and time. Having in mind the experimental finding of high k_f value and very similar transition moments in emission (M_f) and absorption (M_a) (Table 1), we can conclude that, independent of solvent polarity, the emissive singlet state of ADAB is $^1\pi\pi^*$ (CT).

The temporal evolution of low temperature TRF spectra of ADAB recorded in solvents of increasing polarity index—BE, MTHF, and BuCN—can be described by the sequence primary → secondary excited species (P → S) and understood in terms of (i) solvent cage reorganization and (ii) excited state geometry relaxation. Low temperature TRF spectra of ADAB recorded in BE at 203 K (Figure 7B) and BuCN at 173 K (Figure 9B) exhibit a time-dependent shift of their maxima generated by solvent relaxation. Contrary to that, TRF spectra recorded in EE at 203 K[28] and MTHF at 133 K (Figure 8) exhibit dual emission, which indicates that the transformation in the excited state is thermally activated. The detailed investigation performed for ADAB in MTHF indicates that the relaxation of the solvent cage is completed for the primary form along the reaction path and this process is significantly faster than the relaxation of bulk MTHF (Table 3).

Rettig and co-workers[51] reported high (25400 cm^{-1}) and low energy (23000 cm^{-1}) gain (stimulated emission) for the cyano analogue of ADAB in their TA experiment and observed the precursor−successor relationship between the emitting species. These authors observed the same phenomenon in the case of a planar (fluorine-like) model compound. The authors claim that the primary emissive excited state is L_b, and the secondary is of L_a (CT) type; the calculated dipole moments are 8.3 and 15.7 D, respectively. Consistent with the MCD experiment, the results of our calculations for ADAB suggest that the L_b state is located about 4000 cm^{-1} higher than L_a, and, consequently, the interactions between these states should be negligible. These facts eliminate, in the case of ADAB, the model of excited state inversion applied for its cyano analogue.[51] We propose that the complicated photophysics of ADAB can be explained by a scheme involving dynamic stabilization of the $^1\pi\pi^*$ (L_a) with respect to $^1n\pi^*$, as shown in Figure 14. This figure presents the

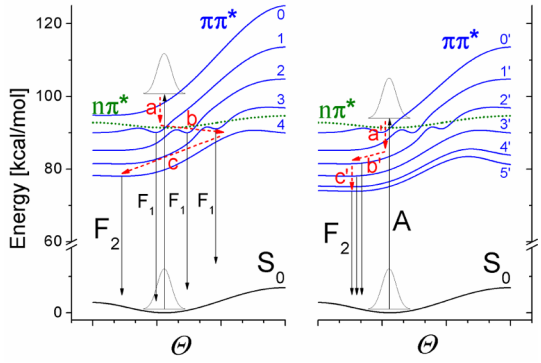

Figure 14. Schematic representation of the temporal evolution of the $^1\pi\pi^*$ (CT) potential energy surface of ADAB due to interaction with a nearby $^1n\pi^*$ state in solvents of lower (left) and higher (right) polarity. Curve 0 is the TD-DFT calculated vertical transition energy. The remaining curves correspond to the stabilization of $^1\pi\pi^*$ by a medium with dielectric constants of ε = 1.5 (1 and 0′), ε = 2.2 (2 and 1′), ε = 3.4 (3 and 2′), ε = 6.0 (4 and 3′), ε = 15.0 (4′), and ε = 37 (5′). See text for details. Red arrows indicate possible relaxation paths. Vertical arrows denote absorption (A) and high (F_1) and low (F_2) energy emission. The barriers on the curves are only schematic and do not reflect the results of calculations.

shape and position of the $^1n\pi^*$and $^1\pi\pi^*$ (L_a) states as a function of Θ based on TD-DFT calculations. Curves 0 and 0′ correspond to the vertical excitation calculated for the ground state optimized geometry. The slope of the curve for $^1\pi\pi^*$ was scaled by a factor of 1.75, so that the destabilization due to twisting is the average of TD-DFT and CIS results; the TD-DFT calculated separation of $^1n\pi^*$ and $^1\pi\pi^*$ was maintained. Another scaling factor (0.69) was used for the calculated Θ dependence of the $^1\pi\pi^*$ dipole moment in order to obtain for the planar structure the value corresponding to that determined experimentally, 18 D. The value of 26 D calculated for the twisted structure was not changed. The remaining curves in Figure 14 were simulated for the $^1\pi\pi^*$ state using the Onsager model: $E(\varepsilon) = E_0 - 2\mu^2F(\varepsilon)/hca_0^3$, where $F(\varepsilon) = (\varepsilon - 1)/(2\varepsilon + 1)$ and a_0 = 6 Å. These curves can be considered as depicting consecutive steps of solvation in a given solvent (time evolution of solvation). The $^1n\pi^*$ state is predicted to have a small dipole moment, practically not dependent on Θ. Its energy also does not change much with Θ and is not expected to be significantly influenced by solvent polarity; therefore, its position is considered constant in Figure 14. On the contrary, the energy of the $^1\pi\pi^*$ (L_a) state decreases with flattening. This state should also be stabilized in polar solvents, due to its large dipole moment. Thus, the stabilization should be both solvent- and temperature-dependent. The stabilization of $^1\pi\pi^*$ (L_a) can be controlled by two factors, intramolecular and solvent relaxation. The latter can be divided into the ultrafast electronic and inertial relaxation (arrows *a* and *a*′ in Figure 14), too fast to be captured with the time resolution of our instruments, and slower processes, involving solvent reorientation. The inter-

DOI: 10.1021/jp510856u
J. Phys. Chem. B XXXX, XXX, XXX−XXX

action between $^1n\pi^*$ and $^1\pi\pi^*$ is the strongest when their energies approach each other. Such a situation may result in a barrier, schematically indicated in Figure 14, of which the magnitude and position would change with time after excitation, due to different stabilization of the two interacting states. The model predicts that, depending on the solvent polarity, the intramolecular relaxation can proceed with or without a barrier; the latter will be true for strongly polar environments. A complex scenario may be realized in solvents not polar enough, where the barrier will exist just after excitation; subsequent stabilization of $^1\pi\pi^*$ will lead to lowering of the barrier or even to switching into a barrierless regime, as shown schematically in Figure 14.

Solvent dependence of the energetics and dynamics of photoinduced charge transfer processes coupled with intramolecular structural changes has been previously analyzed in terms of a two-state model involving locally excited and charge transfer states.[52,53] This model, based on separation of intramolecular and solvation coordinates, was successful in predicting absorption and emission spectra in different solvents. The relative yields of LE and CT emissions, however, could not be reproduced. This was later explained by the formation of photoproducts.[54] Our approach is also based on the interaction between two different electronic states, but the case of ADAB seems too complicated to attempt a quantitative model. First, $^1n\pi^*$ is a dark state, and its position can only be estimated, but not experimentally observed. Second, one cannot make the assumption that one can neglect the distribution over a range of Θ values, as was done by Maroncelli and co-workers in their paper on alkylaminobenzonitriles.[53] Another assumption of that work was that polarizabilities are the same in all three adiabatic states involved. This assumption would be very crude in the case of ADAB. Finally, even though we base our model on the interaction of two close-lying states, we have to be aware about a possible contribution from the second highest $\pi\pi^*$ level.

It would be natural to assume that the intramolecular relaxation coordinate corresponds to the flattening of the excited chromophore, i.e., to the decrease of Θ, as presented in Figure 14. It should be noted, however, that the cyano analogue of ADAB and its planar (Θ = 0°) model compound were reported to exhibit very similar transient absorption dynamics, even though the authors suggested a crucial role of the twisting angle Θ.[51] Our theoretical attempts to find another intramolecular coordinate responsible for excited state relaxation were not successful (Figures S5−S7, Supporting Information).

The starting point of the excited state relaxation path seems to be solvent-independent because in rigid environments the maximum of the emission of ADAB is located at the same spectral position (Table 1). An intriguing difference has been noted in the temporal evolution of fluorescence in solvents of different polarity at lower temperatures. For ADAB in MTHF at 133 K (Figure 8B), the primary fluorescence shifts on the time scale much shorter than the solvent relaxation time (29 vs 200−300 ps, cf. Table 3). Once formed, the low energy band remains at the same position for several hundred picoseconds. In the more polar BuCN at 173 K, the situation is the opposite (Figure 9B). Now, the rapidly formed low energy band is undergoing a red shift, but this time the relaxation time evaluated from the $c(t)$ function, about 90 ps, is in perfect agreement with the literature data (Table 4). The observation that the species responsible for the low energy emission is formed much faster in a more polar BuCN is readily explained by our model. However, the discrepancy between the observed and literature data for MTHF requires further studies. Assuming that the shift of the primary band is due to solvent relaxation, it is not clear which mechanism is responsible for the acceleration of the solvent relaxation in the case of MTHF. A possible explanation would be that the energy transfer from ADAB to the bulk (vibrational cooling) proceeds differently in MTHF and BuCN at low temperatures. In MTHF for a short time interval, this energy is accumulated in the solvent cage and, consequently, the transient local temperature is significantly higher than that of the bulk. Contrary to that, in BuCN, the excess of energy is transferred immediately to the bulk, and therefore, the temperature of the cage and the bulk is the same. Such a hypothesis is consistent with the reported values of thermal conductivities of organic solvents. The data for MTHF are not known, but THF exhibits a smaller conductivity than BuCN.[55]

5. CONCLUSIONS

Both stationary and time-resolved emission of ADAB depend dramatically on solvent polarity. The $S_1 \rightarrow$ TICT excited state reaction path was excluded on the basis of the TA spectra recorded for ADAB in polar environments and on the basis of quantum chemical calculations. Our experimental results, supported by calculations, favor the hypothesis of a flattening of ADAB in the electronically excited state. To explain the temporal evolution of the TRF spectra, a model was introduced that considers dynamic solvent-dependent interaction between two close-lying excited electronic states. In order to assess the role of different intramolecular coordinates in excited state relaxation, further studies are planned, in particular those involving time-resolved infrared spectroscopy.

■ ASSOCIATED CONTENT

Ⓢ Supporting Information

Additional kinetics and spectral data and results of calculations of energy levels as a function of twist and pyramidalization angles. This material is available free of charge via the Internet at http://pubs.acs.org.

■ AUTHOR INFORMATION

Corresponding Authors

*E-mail: dobkowsk@ichf.edu.pl. Fax: (+48 22) 343 3333.
*E-mail: waluk@ichf.edu.pl. Fax: (+48 22) 343 3333.

Present Address

†Central Laser Facility, Research Complex at Harwell, STFC Rutherford Appleton Laboratory, Harwell Science and Innovation Campus, Chilton, Oxfordshire, OX11 0QX, United Kingdom.

Notes

The authors declare no competing financial interest.

■ ACKNOWLEDGMENTS

The authors would like to express gratitude to Dr. Wolfgang Kühnle (Göttingen, Germany) for the synthesis of 4-acetyl-4′-(dimethylamino)biphenyl and 4-acetyl-4′-dimethylamino-2,2′-dimethylbiphenyl, to Andrzej Ardasiewicz for his assistance in software development, and to Dr. Patrycja Kowalska for measuring the MCD spectrum. This work was sponsored by grants 3545/H03/2007/32 from the Polish Committee of Scientific Research and 2011/03/B/ST4/02621 from the Polish National Science Centre and the computing grant

DOI: 10.1021/jp510856u
J. Phys. Chem. B XXXX, XXX, XXX−XXX

G17-14 from the Interdisciplinary Centre for Mathematical and Computational Modeling of the Warsaw University.

REFERENCES

(1) Lippert, E.; Lüder, W.; Boos, H. *Advances in Molecular Spectroscopy*; Pergamon: Oxford, U.K., 1962.
(2) Khalil, O. S.; Hofeldt, R. H.; McGlynn, S. P. Electronic Spectroscopy of Highly-Polar Aromatics. Molecular Interactions in the Ground and Excited States of N,N-Dimethyl-*p*-cyanoanline. *Chem. Phys. Lett.* **1972**, *17*, 479−481.
(3) Khalil, O. S.; Hofeldt, R. H.; McGlynn, S. P. Electronic Spectroscopy of Highly-Polar Aromatics. V. The Polar Excimer of N, N-Dialkyl-*p*-cyanoaniline. *J. Lumin.* **1973**, *6*, 229−244.
(4) Chandross, E. A. *The Exciplex*; Academic Press: New York, 1975.
(5) Visser, R. J.; Varma, C. A. G. O. Source of Anomalous Fluorescence from Solutions of 4-N,N-Dimethylaminobenzonitrile in Polar-Solvents. *J. Chem. Soc., Faraday Trans. 2* **1980**, *76*, 453−471.
(6) Zachariasse, K. A.; von der Haar, T.; Hebecker, A.; Leinhos, U.; Kühnle, W. Intramolecular Charge-Transfer in Aminobenzonitriles - Requirements for Dual Fluorescence. *Pure Appl. Chem.* **1993**, *65*, 1745−1750.
(7) Sobolewski, A. L.; Sudholt, W.; Domcke, W. Ab Initio Investigation of Reaction Pathways for Intramolecular Charge Transfer in Dimethylanilino Derivatives. *J. Phys. Chem. A* **1998**, *102*, 2716−2722.
(8) Zachariasse, K. A. Comment on "Pseudo-Jahn-Teller and TICT-models: a Photophysical Comparison of meta-and para-DMABN Derivatives" [Chem. Phys. Lett. 305(1999)8] - The PICT Model for Dual Fluorescence of Aminobenzonitriles. *Chem. Phys. Lett.* **2000**, *320*, 8−13.
(9) Zachariasse, K. A.; Grobys, M.; von der Haar, T.; Hebecker, A.; Ilichev, Y. V.; Morawski, O.; Ruckert, I.; Kühnle, W. Photoinduced Intramolecular Charge Transfer and Internal Conversion in Molecules with a Small Energy Gap Between S_1 and S_2. Dynamics and Structure. *J. Photochem. Photobiol., A* **1997**, *105*, 373−383.
(10) Cogan, S.; Zilberg, S.; Haas, Y. The Electronic Origin of the Dual Fluorescence in Donor-acceptor Substituted Benzene Derivatives. *J. Am. Chem. Soc.* **2006**, *128*, 3335−3345.
(11) Grabowski, Z. R.; Rotkiewicz, K.; Siemiarczuk, A.; Cowley, D. J.; Baumann, W. Twisted Intra-Molecular Charge-Transfer States (TICT) - New Class of Excited-States with a Full Charge Separation. *Nouv. J. Chim.* **1979**, *3*, 443−454.
(12) Grabowski, Z. R.; Dobkowski, J. Twisted Intramolecular Charge-Transfer (TICT) Excited-States - Energy and Molecular-Structure. *Pure Appl. Chem.* **1983**, *55*, 245−252.
(13) Dobkowski, J.; Kirkor-Kamińska, E.; Koput, J.; Siemiarczuk, A. Excited and Ground-State Conformations of *p*-Dimethylamino-Benzaldehyde and *p*-Dimethylaminoacetophenone. *J. Lumin.* **1982**, *27*, 339−355.
(14) Grabowski, Z. R.; Dobkowski, J.; Kühnle, W. Model Compounds in Study of the Photophysical Behavior of Carbonyl Derivatives of N,N-Dimethylaniline. *J. Mol. Struct.* **1984**, *114*, 93−100.
(15) Dobkowski, J.; Sazanovich, I. The Excited State Relaxation Path of N,N-Diethyl-5-cyanopyridine and N,N-Diethylbenzaldehyde. *Polym. J. Chem.* **2008**, *82*, 831−845.
(16) Dobkowski, J.; Waluk, J.; Yang, W.; Rullière, C.; Rettig, W. Intramolecular Charge-Transfer Properties of a Molecule with a Large Donor Group: The Case of 4′-(1-Pyrenyl) Acetophenone. *New J. Chem.* **1997**, *21*, 429−445.
(17) Dobkowski, J.; Rettig, W.; Waluk, J. Intramolecular Charge-Transfer Properties of a Molecule with a Large Donor Group: the Case of 4 ′-(Pyren-1-yl) benzonitrile. *Phys. Chem. Chem. Phys.* **2002**, *4*, 4334−4339.
(18) Herbich, J.; Kapturkiewicz, A. Electronic Structure and Molecular Conformation in the Excited Charge Transfer Singlet-States of 9-Acridyl and Other Aryl Derivatives of Aromatic Amines. *J. Am. Chem. Soc.* **1998**, *120*, 1014−1029.
(19) Grabowski, Z. R.; Rotkiewicz, K.; Rettig, W. Structural Changes Accompanying Intramolecular Electron Transfer: Focus on Twisted Intramolecular Charge-Transfer States and Structures. *Chem. Rev.* **2003**, *103*, 3899−4031.
(20) Haas, Y.; Zilberg, S.; Dick, B. Conical Intersections and the Electronic Structure of the Excited States of N-Phenyl Pyrrole - a Prototype Molecule Exhibiting Dual Fluorescence. *Polym. J. Chem.* **2008**, *82*, 773−793.
(21) Zgierski, M. Z.; Fujiwara, T.; Lim, E. C. Conical Intersections and ultrafast Intramolecular Excited-State Dynamics in nucleic Acid Bases and Electron Donor-Acceptor Molecules. *Chem. Phys. Lett.* **2008**, *463*, 289−299.
(22) Fujiwara, T.; Lee, J. K.; Zgierski, M. Z.; Lim, E. C. Intramolecular Charge Transfer in The Excited State of 4-Dimethylaminobenzaldehyde and 4-Dimethylaminoacetophenone. *Chem. Phys. Lett.* **2009**, *481*, 78−82.
(23) Maus, M.; Rettig, W. The Electronic Structure of 4-(N,N-Dimethylamino)-4′-cyano-biphenyl and its Planar and Twisted Model Compounds. *Chem. Phys.* **1997**, *218*, 151−162.
(24) Rettig, W.; Kharlanov, V.; Maus, M. Excited-State Relaxation Properties of Ionic and Nonionic Donor-Acceptor Biphenyl Derivatives. *Chem. Phys. Lett.* **2000**, *318*, 173−180.
(25) Herbich, J.; Waluk, J. Excited Charge-Transfer States in 4-Aminopyrimidines, 4-(Dimethylanilino)Pyrimidine and 4-(Dimethylamino)Pyridine. *Chem. Phys.* **1994**, *188*, 247−265.
(26) Szczepanik, B.; Obara, R.; Rothe, A.; Weigel, W.; Rettig, W.; Stachera, M.; Rotkiewicz, K. Enhancement of Photoacidity by Formation of an Intramolecular Charge Transfer State with Twisted Conformation. *Polym. J. Chem.* **2008**, *82*, 807−829.
(27) Dobkowski, J.; Grabowski, Z. R.; Waluk, J.; Kühnle, W.; Rettig, W.; Rullière, C.; Yang, W.; Adamus, J.; Gebicki, J. Excited-State Relaxation Processes in the Case of Some Acetophenone Derivatives. *Proc. - Indian Acad. Sci., Chem. Sci.* **1992**, *104*, 143−152.
(28) Dobkowski, J.; Sazanovich, L. The Geometry of the Excited Charge Transfer States: Flattening or Twisting? *Acta Phys. Pol., A* **2007**, *112*, S127−S142.
(29) Jasny, J. Multifunctional Spectrofluorimetric System. *J. Lumin.* **1978**, *17*, 149−173.
(30) Velapoldi, R. A. National Bureau of Standards Special Publication 378, Accuracy in Spectrophotometry and Luminescence Measurements, Proc. Conf. NBS. Gaithersburg, MD, 1972.
(31) Dobkowski, J.; Galievsky, V. A.; Jasny, J.; Sazanovich, I. V. Time-resolved Emission Spectroscopy of Pyrene Derivatives. *Polym. J. Chem.* **2004**, *78*, 961−972.
(32) Barbara, P. F.; Jarzęba, W. Ultrafast Photochemical Intramolecular Charge and Excited State Solvation. *Advances in Photochemistry*; John Wiley & Sons Inc.: Hoboken, NJ, 1990; Vol. *15*, pp 1−68.
(33) Dreuw, A.; Weisman, J. L.; Head-Gordon, M. Long-Range Charge-Transfer Excited States in Time-Dependent Density Functional Theory Require Non-Local Exchange. *J. Chem. Phys.* **2003**, *119*, 2943−2946.
(34) Yanai, T.; Tew, D. P.; Handy, N. C. A New Hybrid Exchange-Correlation Functional Using the Coulomb-Attenuating method (CAM-B3LYP). *Chem. Phys. Lett.* **2004**, *393*, 51−57.
(35) Peach, M. J. G.; Benfield, P.; Helgaker, T.; Tozer, D. J. Excitation Energies in Density Functional Theory: An Evaluation and a Diagnostic Test. *J. Chem. Phys.* **2008**, *128*, 044118.
(36) Frisch, M. J.; Trucks, G. W.; Schlegel, H. B.; Scuseria, G. E.; Robb, M. A.; et al. *Gaussian 09*, revision B.01; Gaussian, Inc.: Wallingford, CT, 2010.
(37) Bilot, L.; Kawski, A. Zur Theorie des Einflusses von Lösungsmitteln auf die Elektronenspektren der Moleküle. *Z. Naturforsch., A: Phys. Sci.* **1962**, *17*, 621−627.
(38) Liptay, W. *Excited States*; Academic Press: New York, 1974; Vol. *1*.
(39) Lippert, E. Dipolmoment und Elektronenstruktur von Angeregten Molekulen. *Z. Naturforsch., A: Phys. Sci.* **1955**, *10*, 541−545.
(40) Mataga, N.; Kaifu, Y.; Koizumi, M. The Solvent Effect on Fluorescence Spectrum - Change of Solute-Solvent Interaction during

DOI: 10.1021/jp510856u
J. Phys. Chem. B XXXX, XXX, XXX−XXX

the Lifetime of Excited Solute Molecule. *Bull. Chem. Soc. Jpn.* **1955**, *28*, 690−691.
(41) McRae, E. G. Theory of Solvent Effects on Molecular Electronic Spectra - Frequency Shifts. *J. Phys. Chem.* **1957**, *61*, 562−572.
(42) Maus, M.; Rettig, W.; Bonafoux, D.; Lapouyade, R. Photo-induced Intramolecular Charge Transfer in a Series of Differently Twisted Donor - Acceptor Biphenyls as Revealed by Fluorescence. *J. Phys. Chem. A* **1999**, *103*, 3388−3401.
(43) Furutsuka, T.; Imura, T.; Kojami, T.; Kawale, K. *Technol. Rep. Osaka Univ.* **1974**, *24* (1155−1190), 367.
(44) Kearns, D. R.; Case, W. A. Investigation of Singlet - Triplet Transitions by Phosphorescence Excitation Method 0.3. Aromatic Ketones and Aldehydes. *J. Am. Chem. Soc.* **1966**, *88*, 5087−5097.
(45) Bulgarevich, D. S.; Kajimoto, O.; Hara, K. Effect of Pressure on the Conformational Behavior of 4-[4-(Dimethylamino)Phenyl]-Pyridine in the Ground and Fluorescent S_1-Excited States. *J. Phys. Chem.* **1994**, *98*, 2278−2281.
(46) Chou, P.-T.; Chang, C.-P.; Clements, J. H.; Meng-Shin, K. Synthesis and Spectroscopic Studies of 4-Formyl-4′-N,N-dimethylamino-1,1′-biphenyl: The Unusual Red Edge Effect and Efficient Laser Generation. *J. Fluoresc.* **1995**, *5*, 369−375.
(47) Dähne, S.; Freyer, W.; Teuchner, K.; Dobkowski, J.; Grabowski, Z. R. Dual and Multiple Fluorescence Mechanisms of para-Dimethylaminobenzaldehyde and Its Trimethylene-Bridged Double Molecule. *J. Lumin.* **1980**, *22*, 37−49.
(48) Marchetti, A. P.; Kearns, D. R. Investigation of Singlet-Triplet Transitions by Phosphorescence Excitation Method 0.4. Singlet-Triplet Absorption Spectra of Aromatic Hydrocarbons. *J. Am. Chem. Soc.* **1967**, *89*, 768−777.
(49) Lower, S. K.; El-Sayed, M. A. Triplet State and Molecular Electronic Processes in Organic Molecules. *Chem. Rev.* **1966**, *66*, 199−241.
(50) Ernsting, N. P.; Kovalenko, S. A. In Photoinduced Charge (Electron and Proton) Migration Workshop, Wdzydze 2004, Poland.
(51) Maus, M.; Rettig, W.; Jonusauskas, G.; Lapouyade, R.; Rullière, C. Subpicosecond Transient Absorption of Donor-Acceptor Biphenyls. Intramolecular Control of the excited State Charge Transfer Processes by a Weak Electronic Coupling. *J. Phys. Chem. A* **1998**, *102*, 7393−7405.
(52) Tominaga, K.; Walker, G. C.; Jarzęba, W.; Barbara, P. F. Ultrafast Charge Separation in ADMA: Experiment, Simulation, and Theoretical Issues. *J. Phys. Chem.* **1991**, *95*, 10475−10485.
(53) Dahl, K.; Biswas, R.; Ito, N.; Maroncelli, M. Solvent Dependence of the Spectra and Kinetics of Excited-State Chrge Transfer in Three (Alkylamino)benzonitriles. *J. Phys. Chem. B* **2005**, *109*, 1563−1585.
(54) Druzhinin, S. I.; Galievsky, V. A.; Zachariasse, K. A. Photoproduct Formation with 4-Aminobenzonitriles in Acetonitrile and Its Effect on Photophysical Measurements. *J. Phys. Chem. A* **2005**, *109*, 11213−11223.
(55) Kauffman, G. W.; Jurs, P. C. Prediction of Surface Tension, Viscosity, and Thermal Conductivity for Common Organic Solvents Using Quantitative Structure-Property Relationships. *J. Chem. Inf. Comput. Sci.* **2001**, *41*, 408−418.
(56) Polimeno, A.; Barbon, A.; Nordio, P. L.; Rettig, W. Stochastic-Model for Solvent-Assisted Intramolecular Charge-Transfer. *J. Phys. Chem.* **1994**, *98*, 12158−12168.
(57) Meng, X. Y.; Wu, J. T.; Liu, Z. G. Viscosity and Density Measurements of Diisopropyl Ether and Dibutyl Ether at Different Temperatures and Pressures. *J. Chem. Eng. Data* **2009**, *54*, 2353−2358.
(58) Wohlfarth, C. *Viscosity of pure organic liquids and binary liquid mixtures*; Springer-Verlag: Berlin and Heidelberg, 1999.
(59) Richert, R.; Stickel, F.; Fee, R. S.; Maroncelli, M. Solvation Dynamics and the Dielectric Response in a Glass-Forming Solvent - from Picoseconds to Seconds. *Chem. Phys. Lett.* **1994**, *229*, 302−308.
(60) Richert, R.; Angell, C. A. Dynamics of Glass-Forming Liquids. V. On the link between Molecular Dynamics and Configurational Entropy. *J. Chem. Phys.* **1998**, *108*, 9016−9026.
(61) Zhu, X.; Farrer, R. A.; Zhong, Q.; Fourkas, J. T. Orientational Diffusion of *n*-Alkyl cyanides. *J. Phys.: Condens. Matter* **2005**, *17*, S4105−S4118.
(62) Druzhinin, S. I.; Galievsky, V. A.; Yoshihara, T.; Zachariasse, K. A. Intramolecular Charge Transfer and Dielectric Solvent Relaxation in *n*-propyl Cyanide N-phenylpyrrole and 4-Dimethylamino-4 ′-cyanostilbene. *J. Phys. Chem. A* **2006**, *110*, 12760−12768.

DOI: 10.1021/jp510856u
J. Phys. Chem. B XXXX, XXX, XXX−XXX